# Novel Easy to Synthesize Benzonitrile Compounds with Mixed Carbazole and Phenoxazine Substituents Exhibiting Dual Emission and TADF Properties

Antonio Maggiore, Yangyang Qu, Régis Guillot, Piotr Pander, Marharyta Vasylieva, Przemyslaw Data, Fernando Dias, Pierre Audebert, Gilles Clavier, Fabien Miomandre

# Novel Easy to Synthesize Benzonitrile Compounds with Mixed Carbazole and Phenoxazine Substituents Exhibiting Dual Emission and TADF Properties

Antonio Maggiore,[1] Yangyang Qu,[1] Régis Guillot,[2] Piotr Pander,[3,4] Marharyta Vasylieva,[5] Przemyslaw Data,[3,4] Fernando B. Dias,[3] Pierre Audebert,[1] Gilles Clavier,[1]* and Fabien Miomandre[1]*

[1] Université Paris-Saclay, ENS Paris-Saclay, CNRS, PPSM, 91190 Gif-sur-Yvette, France

[2] Université Paris-Saclay, CNRS, ICMMO, 91405 Orsay, France

[3] Department of Physics, University of Durham, DH1 3LE Durham, U.K.

[4] Centre for Organic and Nanohybrid Electronics, Silesian University of Technology, 44-100 Gliwice, Poland

[5] Centre of Polymer and Carbon Materials of the Polish Academy of Sciences, 41-819 Zabrze, Poland

*J. Phys. Chem. B* **2022**, *126*, 2740−2753 DOI: 10.1021/acs.jpcb.2c00219

Received: January 11, 2022; Revised: March 15, 2022: Published: March 30, 2022

**ABSTRACT:** The photophysical and electrochemical properties of a new class of fluorinated benzonitrile compounds substituted with mixed phenoxazine and carbazole units have been investigated. When absorbing in a large range of the UV−vis spectrum due to both localized and charge-transfer absorptions, these compounds show dual broad emission in solution and intense emission in PMMA films, with photoluminescence quantum yields changing from a few percent in solution to 18% in a more rigid environment. The compounds also exhibit thermally activated delayed fluorescence demonstrated by the role of oxygen in the quenching of delayed fluorescence and by time-resolved luminescence studies, with an efficiency directly related to the number of phenoxazine substituents. Electrochemistry reveals dramatic changes in the reduction mechanisms according to the number of remaining fluorine atoms on the benzonitrile core. All these results demonstrate how it is possible to tune the photophysical and electrochemical properties of easily synthesizable derivatives by controlling the nature and relative number of the substituents on a simple aromatic platform.

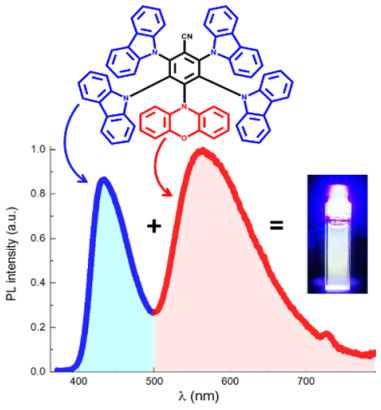


## INTRODUCTION

Nowadays there is a growing demand for efficient white-light-emitting organic molecules due to their applications in lighting and display technologies. In order to achieve natural illumination properties, resembling daylight, a key factor is to cover the entire visible emission range, that is, 400−700 nm.[1,2] The most commonly reported white-light organic emitters consist in a combination of different compounds

that emit in a different range of wavelengths. However, the replacement of multicomponent emitters with a single white-light-emitting molecule would be advantageous in several aspects, for example, improved stability and reproducibility and simpler fabrication process.[3,4]

Efficient thermally activated delayed fluorescence (TADF) emitters with donor–acceptor (D–A) architectures are considered to date among the most promising materials in lighting applications due to their free-metal efficient triplet harvesting properties. The photoluminescence (PL) spectra originating from intramolecular charge-transfer (CT) excited states typical of these materials are significantly broadened in respect to the well-structured and narrowband emission from localized states (LE) in typical non-intramolecular CT fluorescent materials. Moreover, D–A design is crucial for facilitating a very small singlet–triplet ($^1$CT–$^3$CT–$^3$LE) energy gap.[5–7] This ensures an efficient triplet to singlet reverse intersystem crossing (RISC) interconversion that is fundamental to achieve a highly efficient TADF process.[8–10] Another characteristic of TADF active D–A systems is their ability of tuning the emission properties by changing the position or the number of substituents.[9,11] Based on these design principles, various purely organic TADF emitters have been developed. However, to date, one of the most promising strategies to achieve a broadband TADF emission, sufficient to cover the entire visible range, is to take advantage of intermolecular CT exciplex states.[12,13] Nevertheless, even if exciplexes are considered good candidates for lighting application, the use of a single emitter is more advantageous than two or more, as required in exciplexes. Moreover, in some cases, exciplex systems facilitate triplet–triplet annihilation[14] leading to triplet harvesting losses. It results that despite TADF molecules being considered to be the next-generation luminescent materials, the research for single-component white-light TADF materials remains a true challenge.

In this work, we designed and studied the photophysical properties of several new benzonitrile derivatives substituted by carbazole (Cz) and phenoxazine (PhOx) units (Scheme 1). All the molecules are based on a central benzonitrile (BzN) core decorated with a variable number of PhOx and Cz donor substituents and fluorine atoms in the remaining positions. Three series are considered according to the number of PhOx substituents which varies from 1 (series 1) to 3 (series 3).

The use of the electron-deficient BzN core as the acceptor was motivated by the good photophysical properties and the simple synthetic protocols making BzN one of the most popular electron acceptor for constructing TADF molecules since their introduction in the field.[15–22] On the side of donors, Cz was chosen due to its weak donor properties and a relatively low-lying HOMO level, which is a necessary prerequisite for the design of deep-blue TADF emitters.[23] On the contrary, PhOxs possess a strong electron donor character, due to the presence of two heteroatoms (N and O) that are electron-rich and contribute to the HOMO with their non-bonding electrons. This results in a low ionization potential that allows obtaining red-shifted emission.

The use of the BzN core as an acceptor and the mixing of two donor groups in different proportions in the same molecule results in an original molecular design for novel D–A derivatives. Only a few examples of D1–A–D2 TADF compounds have already been reported in the literature[24–30] and therefore we consider it interesting to explore in deep the characteristics of these systems. Our study presents the crystallographic, electrochemical, and photophysical properties of the three series of compounds. The study is mainly focused on the behavior of the 1st series whereas the results concerning the 2nd and 3rd series are reported in the Supporting Information.

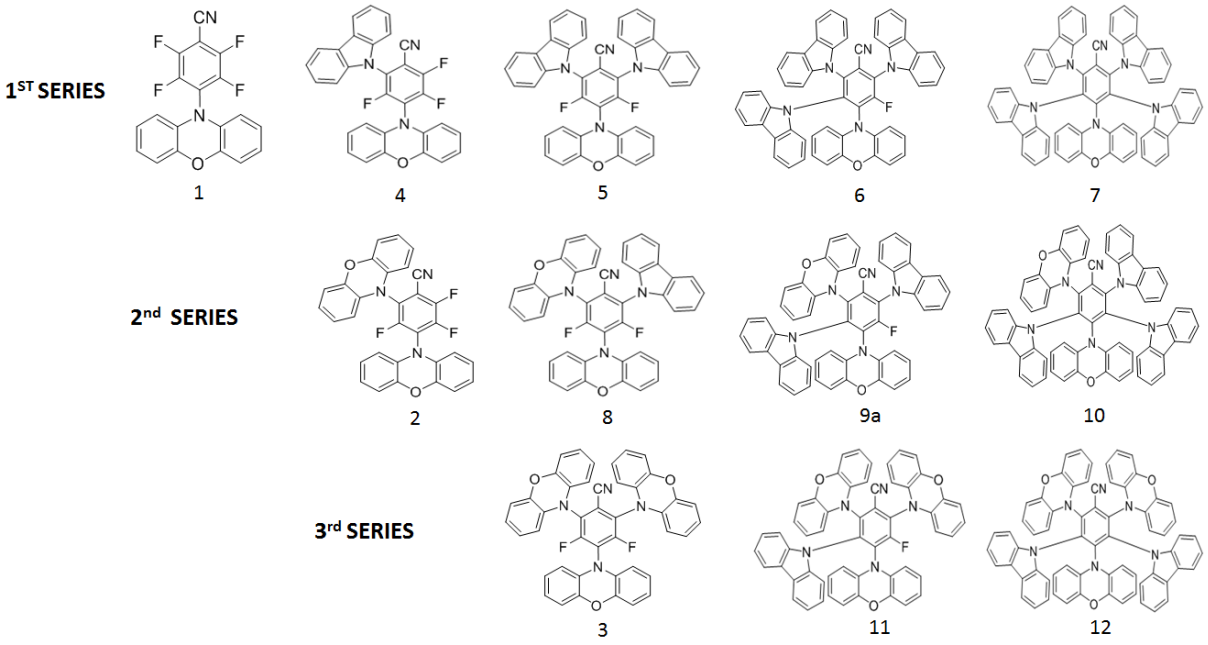


***Scheme 1:*** The three series of polysubstituted fluorobenzonitrile derivatives studied with one (1st series), two (2nd series) and three (3rd series) phenoxazine units and a variable number of carbazole moieties.

## METHODS

*Synthesis and Characterization.* All chemicals were received from commercial sources and used without further purification. Thin layer chromatography (TLC) was performed on silica gel. Column chromatography was performed with SDS 0.040−0.063 mm silica gel. All mixtures of solvents are given in v/v ratio. NMR spectra were recorded on a JEOL ECS (400 MHz) spectrometer. $^{13}C$ NMR spectra were proton decoupled. HRMS spectra were measured either on an UPLC/ESI-HRMS device (Acquity Waters UPLC system coupled to a Waters LCT Premier XE mass spectrometer equipped with an electrospray ion source) or a Q-TOF mass spectrometer (QTOF 6540, Agilent) equipped with an APPI ion source.

*Electrochemistry.* The electrochemical cell is composed of a platinum electrode of 2 mm diameter as a working electrode, an $Ag|Ag^+$ electrode as a reference electrode, and a platinum coil as an auxiliary electrode. Measurements were conducted at room temperature at a potential scan rate of 50 mV/s and were calibrated against a ferrocene/ferrocenium redox couple. Electrochemical measurements were conducted with a CHI600B potentiostat device, in 1.0 mM concentration of all compounds with 0.1 M solutions of Bu4NPF6, 99% (Sigma-Aldrich) added in dichloromethane (DCM) CHROMASOLV, 99.9% (Sigma-Aldrich).

*Quantum Chemical Calculations.* Ground-state geometries were optimized at the B3LYP/6-31+g(d) level of calculation followed by a frequency calculation. TDDFT on these geometries were done at the M06-2X/6-311+g(d,p) level of theory looking for both singlet and triplet levels in vacuo and including the toluene solvent effect with an IEFPCM model. Then, first singlet excited-state geometries were optimized at the M06-2X/6-31+g(d) level followed by a frequency calculation at the same level. Finally, a TDDFT calculation was done on these S1 optimized geometries at the M06-2X/6-311+g(d,p) level of theory looking for both singlet and triplet levels in vacuo and including the toluene solvent effect with an IEFPCM model. In parallel, first triplet excitedstate geometries were optimized at the M06-2X/6-31+g(d)

level followed by a frequency calculation at the same level and by a TDDFT calculation on these T1 optimized geometries at the M06-2X/6-311+g(d,p) level of theory. All calculations were done with Gaussian 16 (Revision B.01) software.[46] Data were analyzed with GaussView 6.0, PyMOL (The PyMOL Molecular Graphics System, Version 2.1.1 Schrödinger, LLC), Mercury 4.1.0, and GaussSum3.0[47] softwares. Calculated absorption spectra were obtained by a convolution of Gaussian functions with a 3000 $cm^{-1}$ (0.37 eV) FWHM.

*Film Processing.* All blends were obtained by drop-casting DCM solutions (0.05 g/L) of the compounds at room temperature on quartz slides followed by slow (1 night) evaporation under solvent-saturated conditions. Concentration of the fluorophore in the film is reported in weight percentage (w/w) relative to the polymer mass in the solution. All blends formed clear, glassy, and transparent solid films.

*Photophysical Studies.* UV−vis absorption measurements (scan mode) were collected using a Cary 4000 double beam spectrophotometer (Agilent) using rectangular 10 mm path length quartz cuvettes from Hellma, at 25 °C. The absorption spectra were recorded with concentrations in the range of 5.6−2.0 μM (total volume = 10 mL volumetric flask). For all the solvents, dilutions were made from a stock solution in chloroform at 1 mg/5 mL.

Fluorescence spectroscopic studies were performed with a FluoroLog3 fluorescence spectrometer (Horiba Jobin Yvon) at 25 °C, with rectangular 10 mm path length quartz cuvettes from Hellma. The emission and excitation spectra were recorded with a diluted solution with absorbance lower than 0.1. For the excitation and emission spectra, the slit widths were adjusted between 2 and 5 nm, integration time = 0.1 s, and 1 nm step. All fluorescence spectra were corrected from the lamp fluctuations and the apparatus response fluctuations.

The relative photoluminescence quantum yield (PLQY) in solution were determined at 25 °C, from corrected emission spectra using quinine sulfate in 0.1 M HClO4 as a standard.[48] For each PLQY measurement, slit width, excitation wavelength, scan rate, integration time, and emission range were kept identical for the reference and the sample. PLQY was determined thanks to the following formula

$$\Phi_S = \Phi_R \bullet \left(\frac{Abs_R}{Abs_S}\right) \bullet \left(\frac{\eta_S^2}{\eta_R^2}\right) \bullet \left(\frac{I_S}{I_R}\right)$$

where Φ = PLQY, Abs = absorbance of the solution, η = refractive index of the solvent, I = integrated fluorescence intensity of the emitted light, and subscripts “R” and “S” refer to the reference and the sample, respectively.

Lifetime experiments were done using 10 mm path length quartz cuvettes: The ns fluorescence decay curves in solution were obtained by the time-correlated single-photon counting method with a femtosecond laser excitation composed of a titanium sapphire laser (Tsunami, Spectra-Physics) pumped by a doubled Nd:YVO4 laser (Millennia Xs, Spectra-Physics). The fluorescence data were analyzed using the Globals software package developed at the Laboratory for Fluorescence Dynamics at the University of Illinois at Urbana-Champaign, which includes reconvolution analysis and the global nonlinear least-squares minimization method. The quality of the fit was estimated by visual inspection of the weighted residuals and calculation of $\chi^2$.

The μs fluorescence decay curves in solution were obtained using an Edinburgh instrument LP920 laser flash photolysis spectrometer combined with a Nd:YAG laser (continuum) tripled at 355 nm via non-linear crystals. The Levenberg Marquardt algorithm was used for non-linear least-squares fit (tail fit) as implemented in the L900 software (Edinburgh instrument). The quality of the fit was estimated by visual inspection of the weighted residuals and calculation of $\chi^2$.

**RESULTS AND DISCUSSION**

*Synthesis.* Scheme 2 summarizes the first synthetic steps for these new compounds. The different reactivities of the five fluorine atoms on pentafluorobenzonitrile (PFBN) toward nucleophilic substitution offer a special advantage to prepare various symmetrically and unsymmetrically substituted BzN derivatives in a facile manner. The para fluorine atom, and to a lesser extent the ortho ones, of PFBN readily undergo nucleophilic substitution selectively in a dipolar aprotic solvent (DMF) and in the presence of a weak base ($K_2CO_3$) at room temperature, with the moderate nucleophilic anion issued from the PhOx. This way, compounds **1**, **2**, and **3** were easily synthesized by sequential nucleophilic displacement of the para, ortho, and ortho' fluorine atoms on PFBN using 1, 2, or 3 equiv of PhOx, respectively, giving in each case the targeted compound quantitatively.

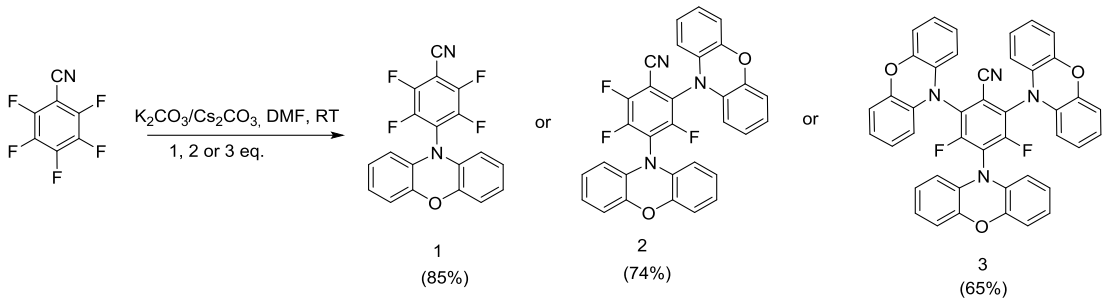


***Scheme 2***: Substitution of fluorine atoms on PFBN with 1, 2 or 3 eq. of phenoxazine anion.

The meta and meta' fluorine atoms can be substituted as well but by stronger nucleophiles, which provides a possible opportunity for the synthesis of heterosubstituted compounds. In this work, we decided to use a carbazolyl anion as such a nucleophile. Compounds 4−12 were successfully prepared by further reaction of compounds **1**, **2**, and **3** with the nucleophile. The remaining fluorine atoms were displaced sequentially with various equivalents of Cz in the presence of $K_2CO_3$ or $Cs_2CO_3$ at room temperature or at 60−80 °C, according to the reactivity of the compounds. We link the latter to the steric hindrance generated by the PhOx already connected to the BzN core in addition to the intrinsic reactivity of the fluorine atoms as a function of their position on PFBN (Scheme 3). This difference in reactivity between the PhOx and Cz anions allowed us to prepare most of the mixed and partially and fully substituted BzNs reported here.

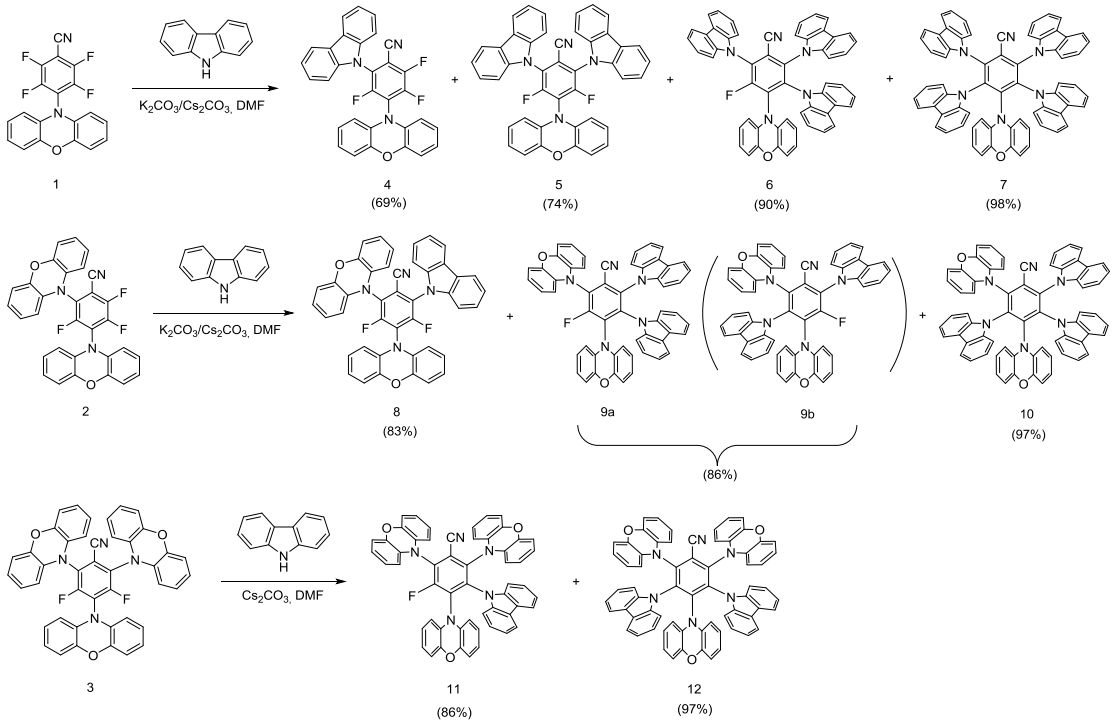


***Scheme 3:*** Synthesis of the various heterosubstituted compounds by displacement of fluorine by carbazole.

As long as the reaction conditions are carefully controlled, the sequential substitution reactions proceed smoothly resulting in the target substituted compound as the main product, with only small amount of side products featuring other substitutions. In the case of compound **9**, **9b** was always obtained in ca. 10% amount, along with the major isomer **9a**. All products were purified by column chromatography and characterized by $^{19}F$, $^{1}H$, and $^{13}C$ NMR spectroscopy and mass spectrometry (see the Experimental Section and Supporting Information for details).

*X-ray Diffraction Analysis.* Geometries of the selected BzN derivatives were obtained from single crystal X-ray diffraction (XRD). Only crystal structures of **1** and **4–7** were obtained and are presented in Figure 1A (see all crystallographic data reported in Table S1). All the molecules show large twisting angles between the donor and acceptor moieties, a beneficial situation to get spatial separation of the HOMO and LUMO and a small singlet−triplet energy gap which is a necessary condition to obtain TADF properties. The D−A dihedral angles tend to decrease with the increasing number of donor moieties on the BzN core (see Table S2). Moreover, the dihedral angles between PhOx and the acceptor unit are in general larger than those involving Cz.

DFT calculations have been performed on compounds **1–12** to predict the optimized geometries of these molecules. Figure 1B shows the overlap of crystal structures and calculated ground-state geometries. The angles between the main planes of Cz and PhOx obtained from XRD structures match quite well with the calculated ones in the ground state (Table S2), especially for the molecules with the lower number of substituents (**1, 4, 5**).

*Energy Levels, Molecular Orbitals, and Electrochemistry*. The calculated energies of the molecular orbitals in **1** and **4–7** are presented in Figure 2. The HOMO level gradually increases with the number of Cz units, as expected due to its donor character. The LUMO level increases as well in the same order leading to a

small variation of the HOMO−LUMO gap in the series. The HOMO−LUMO gap is, however, smaller in **7** than in **1**. A similar trend is observed for the 2nd series, whereas the HOMO and LUMO levels remain fairly constant in the 3rd series (Figure S1).

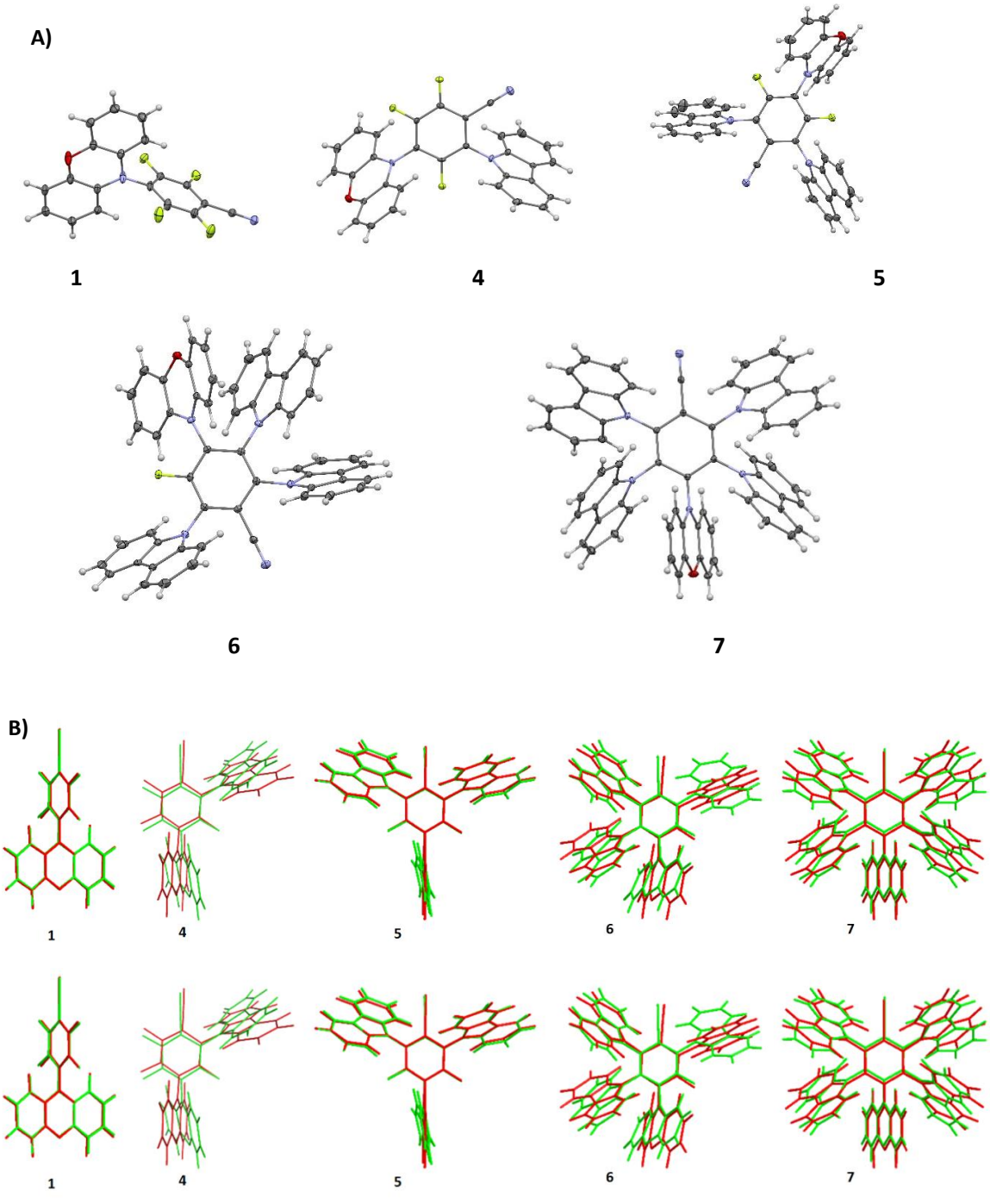


***Figure 1:*** A): ORTEP drawing of compounds **1, 4-7**. Thermal ellipsoids are shown at the 30% level. For the sake of clarity, solvent molecule is omitted and only one molecule of the asymmetric unit in **5** is shown. B): Overlap between ground state calculated (red) and XRD structures (green) for molecules **1** and **4-7**.

Figure 2 also shows the frontier orbital contours of **1** and **4–7**. It is clear that the two highest occupied molecular orbitals (HOMO and HOMO − 1) are centered on PhOx and Cz substituents, whereas the two lowest unoccupied orbitals (LUMO and LUMO − 1) are centered on the BzN. This confirms that D and A subunits are actually electronically independent in all compounds of the 1st series. In a more detailed view, one can see that HOMOs are centered on PhOx and (HOMO-1)s on Cz. One can thus expect the first oxidation to involve PhOx and the second one Cz which will be indeed confirmed by the electrochemical study (see below). The reduction process should mainly concern the BzN core because it is where the LUMO is mainly localized.

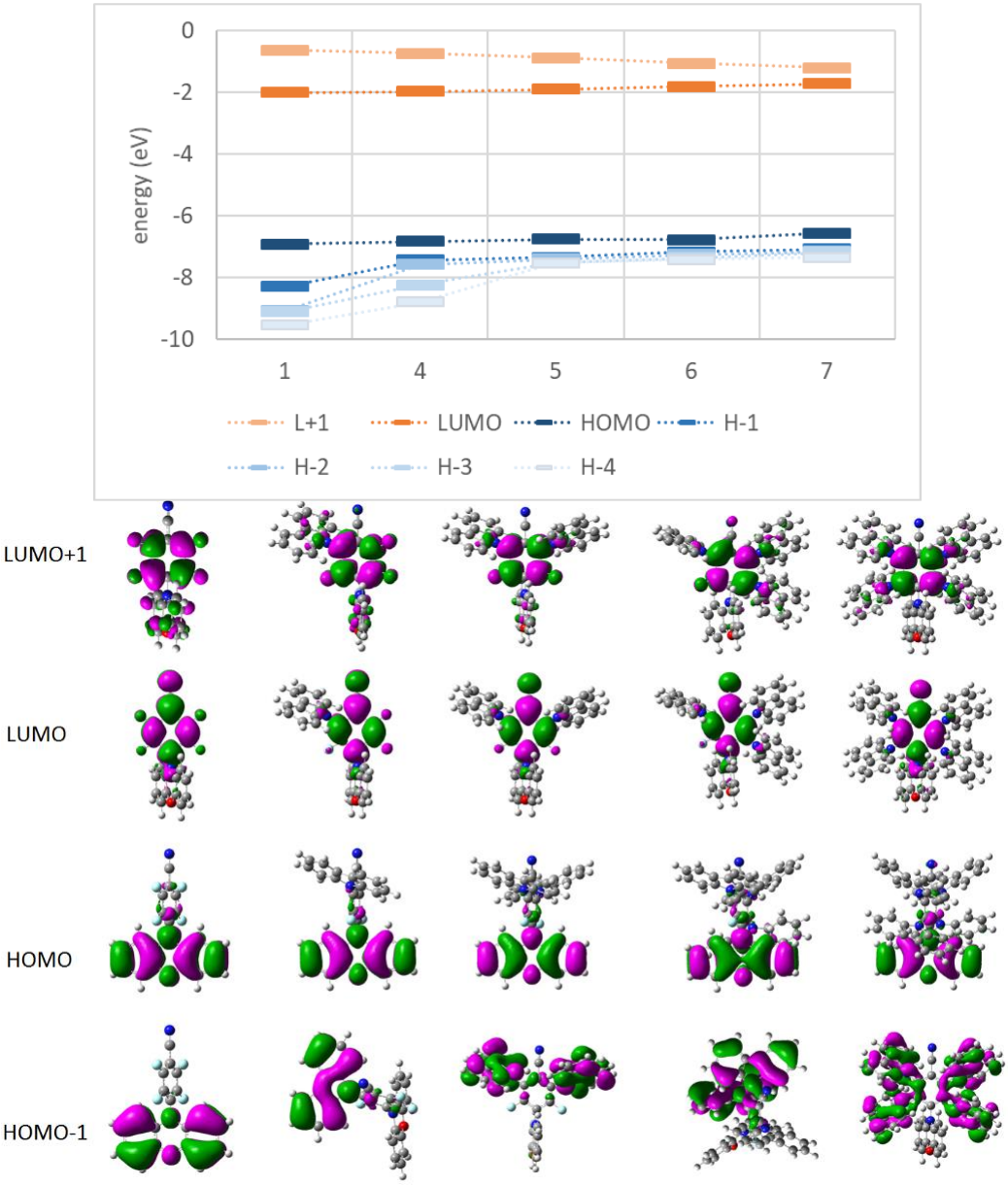


***Figure 2:*** Energy levels and molecular orbital contours of HOMO-1, HOMO, LUMO and LUMO+1, for 1 and 4-7 (from left to right).

Cyclic voltammetry (CV) experiments have been performed on all molecules **1–12** and the results are displayed in Figure 3 for the 1st series and in Figure S3 for the two others.

All CVs feature a cathodic peak which can be assigned to the BzN core reduction and one or more oxidation peaks assigned to the peripheral donor moieties (Cz or PhOx). It is important to note that PhOx is reversibly oxidized, whereas the oxidation of unsubstituted Cz is usually irreversible,[31] sometimes leading to electropolymerization (see Figure S4 for 5). Therefore, compounds **1–3** show a single reversible oxidation assigned unambiguously to PhOx. For the other heterosubstituted BzN compounds, only the first oxidation waves are reversible because the more electron-rich PhOx moieties are always oxidized before the Cz unit.

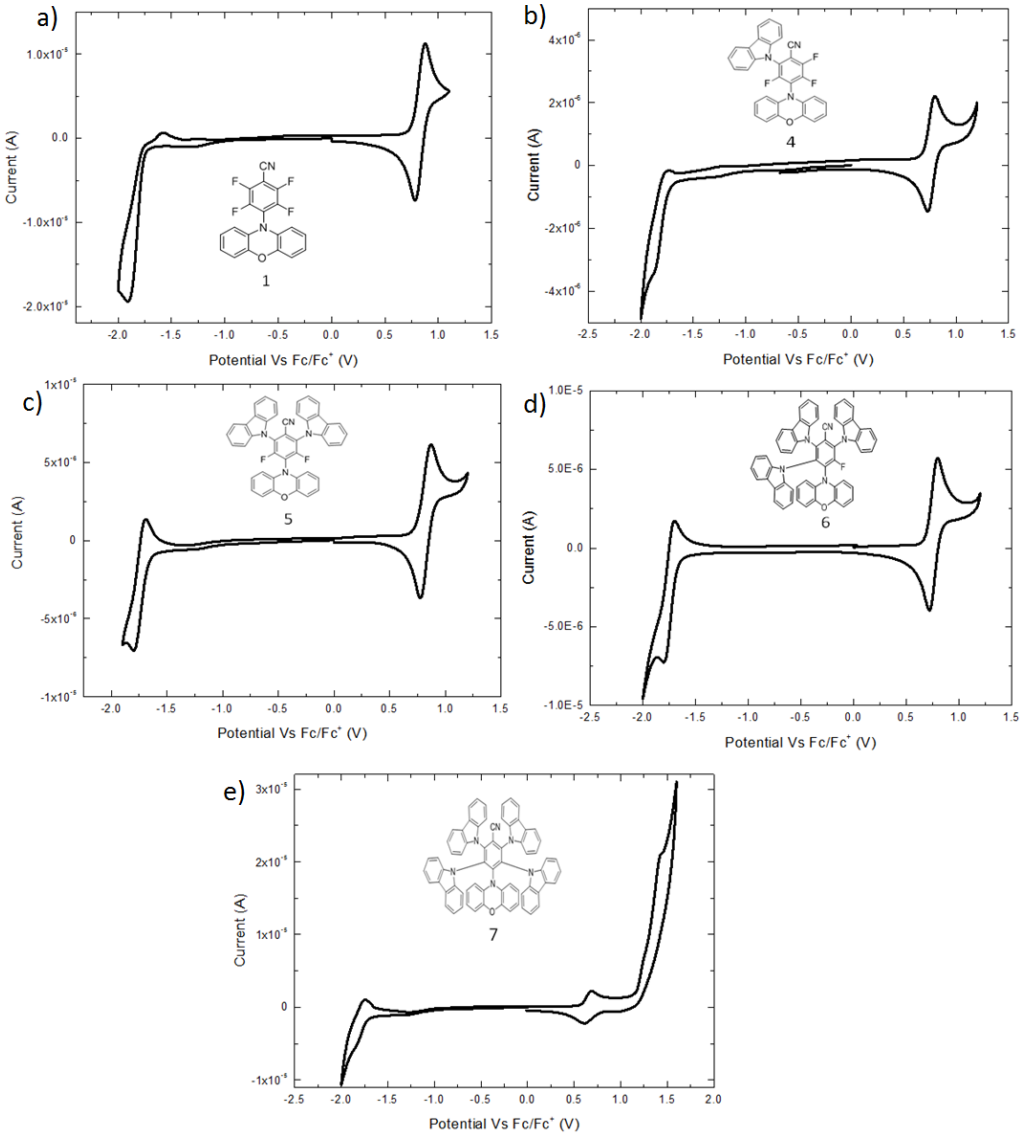


***Figure 3:*** CV traces of compounds **1, 4-7** in dichloromethane (DCM) containing 0.1 M $TBAPF_6$. Scan rate: 50 mV/s.

Interestingly, the reduction of the BzN core gives an irreversible peak for some derivatives and a reversible one for others. A clear trend is visible in Figure 3, where the reversibility gradually appears and increases as the number of fluorine atoms decreases. We can reasonably assume that the lack of reversibility is related to a chemical reaction associated with the electron uptake. When the number of fluorine atoms decreases, the reversibility increases suggesting that fluorine plays the role of a leaving group in the electrochemical reduction process. Besides, the peak current ratio calculated between the first oxidation and the first reduction varies from about 0.6−1 in the 1st series (see Table 1). As the first anodic peak corresponds to the one-electron oxidation of PhOx, one can deduce that the reduction of BzN involves either two electrons (e.g., for 1) or only one (e.g., for 7). A confirmation of this change in the number of electrons exchanged upon reduction according to the number of fluorine atoms on the benzonitrile core is given in Figure S2 by looking at compound **2**, for which the peak ratio is close to 1 because the first oxidation involves this time two electrons (one per PhOx, each behaving independently), the reduction of **2** is thus bielectronic again, as for 1. To be consistent with a bielectronic reduction, the reduction mechanism should lead to either the substitution of fluorine by hydrogen through an ECEC mechanism[32] or to a dimer through an EC2 mechanism,[33] both mechanisms starting by the formation of an intermediate anion radical of fluorobenzonitrile[34] (see figure S5). In absence of fluorine (compound **7**), no leaving group can be removed after the first monoelectronic reduction and the reduction stops at the anion radical level. Interestingly, this is also the case for **6** despite it containing one fluorine atom. We can thus infer that the preferred mechanism is dimerization, which is hampered in **6** due to steric hindrance. It is worth mentioning that the same behavior is observed in the two other series with an irreversible reduction for **2**, a partially reversible reduction for **3**, and a fully reversible reduction for **9–10** and **11–12**.

***Table 1***: Electrochemical data of **1-12**: first peak oxidation and first peak reduction potentials, first anodic *vs*. cathodic peak current ratios, HOMO and LUMO energies derived from CV.

| **Compound** | **$E_{ox}$ vs Fc/Fc$^+$ (V)[(a)]** | **$E_{red}$ vs Fc/Fc$^+$(V)[(a)]** | **Red vs. Ox peak current ratio** | **HOMO (eV)[(b)]** | **LUMO (eV)[(c)]** | **HOMO-LUMO gap (eV)** |
|---|---|---|---|---|---|---|
| **1** | 0.56 | -1.95 | 0.6 | -5.66 | -3.16 | 2.50 |
| **2** | 0.56 | -1.85 | 1.2 | -5.66 | -3.25 | 2.41 |
| **3** | 0.57 | -1.80 | 1.3 | -5.67 | -3.30 | 2.37 |
| **4** | 0.56 | -1.87 | 0.7 | -5.66 | -3.23 | 2.43 |
| **5** | 0.57 | -1.83 | 0.9 | -5.67 | -3.27 | 2.40 |
| **6** | 0.52 | -1.78 | 0.8 | -5.62 | -3.32 | 2.30 |
| **7** | 0.40 | -1.89 | 1.2 | -5.50 | -3.21 | 2.29 |
| **8** | 0.58 | -1.81 | 1.4 | -5.68 | -3.29 | 2.39 |
| **9a** | 0.51 | -1.84 | 1.3 | -5.61 | -3.26 | 2.35 |
| **10** | 0.42 | -1.87 | 0.9 | -5.52 | -3.23 | 2.29 |
| **11** | 0.49 | -1.81 | 1.4 | -5.59 | -3.29 | 2.36 |
| **12** | 0.39 | -1.83 | 0.9 | -5.49 | -3.27 | 2.29 |

(a) Measured in DCM at room temperature by cyclic voltammetry; (b) Estimated from the oxidation potential in DCM, HOMO(/eV) = -Eox (/V) −5.1; (c) Estimated from the reduction potential in DCM, LUMO(/eV) = -Ered(/V) − 5.1.

It is possible also to notice that the reduction potential shifts slightly toward more positive values when substituting fluorine by Cz, especially in the 1st series (Table 1). This is not in agreement with the electron donor effect of Cz compared to the attracting inductive effect of fluorine, nor with the variation of the LUMO energies in the 1st series (Figure 2), but one must consider the role of the chemical reaction following the first electron transfer, which facilitates the reduction and thus tends to shift the potential toward more positive values. The fact that the more substituted compounds in a series are more easily reduced does not allow to discriminate between the two mechanisms. Indeed, the elimination of fluoride in the ECEC mechanism should be favored in the presence of donor substituents such as Cz or PhOx when those substitute the fluorine and thus would lead to the observed positive shift of the reduction potential. However, a strong argument to support the dimerization mechanism as the first reduction step is that non-activated fluoride elimination from a negatively charged species (typically a carbanion) is usually a (very) slow process in organic chemistry and sometimes cannot occur at all ($CF3^-$ is quasi-stable).[35] Therefore, it is highly probable that elimination is extremely slow on the polyfluorinated anion radical and can only occur after the dimerization step because at this point it allows restoration of the aromatic character of the biphenyl ring. The dimerization process is, however, not possible for compounds bearing only one fluorine (**6, 9, 11**) because of steric hindrance and even those bearing two fluorines (**5, 8, 3**) show a partial reversibility, indicating that dimerization as well as ECEC are both slowed down albeit for different reasons.

Regarding the oxidation of the investigated compounds, the first oxidation potential varies slightly in the 1st series, decreasing from **4** to **7**, in agreement with the opposite variation of the HOMO energies (Figure 2). When the investigated compounds involve more than two PhOx, the oxidation wave splits into two or three peaks, due to coulombic repulsion between the injected positive charges. The presence of electron-rich Cz on the BzN core tends to slightly diminish the oxidation potential of PhOx (see **7, 10, 12** compared to **1, 2** in Table 1). Each PhOx behaves as a more or less independent redox unit, and one can also emphasize the generation of a very stable cation radical related to the antiaromatic character of the neutral form for this family of compounds.

*UV−Vis Absorption Properties.* We first show the results of calculated absorption spectra for the 1st series obtained from TDDFT (Figure 4 and Table S3). Three main absorption bands can be observed in each spectrum that can be assigned to either locally excited (LE) or CT excitations. The transitions at lower energy present a CT character. In particular, the lowest energy transition can be assigned to the CT between PhOx and BzN in all cases and is reported further as “PhOx CT”. When Cz moieties are added, additional CT transitions involving Cz as donors appear in between ($\lambda \approx 300-350$ nm) and are reported further as “Cz CT”. All the higher-energy transitions show larger oscillator strengths and are assigned to $\pi-\pi^*$ transitions (LE). All the transitions with their corresponding orbital contributions are listed in Table S3.

The calculated absorption spectra for compounds of the 2nd and 3rd series are shown in Figure S2 (TDDFT results in Table S3). It can be noticed that **2** and **3** present only two distinct CT bands, whereas molecules **8−10** and **11−12** present three, with the same assignment as for the 1st series.

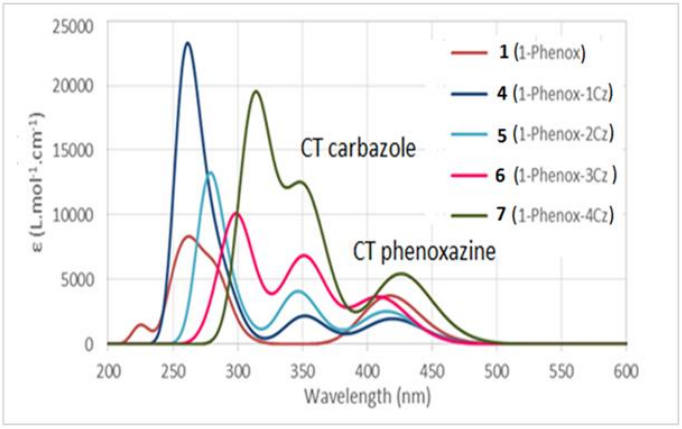


***Figure 4:*** Calculated spectra (DFT) in toluene for the compounds of the 1st series.

Experimental absorption spectra have been recorded for the molecules either in solution ($10^{-5}$ M) with solvents of various polarities or in a PMMA matrix (0.05 wt %). Absorption spectra of **1** and **4–7** in cyclohexane and PMMA are displayed in Figure 5 and the absorption maximum wavelengths are reported in Table 2. The less intense bands at lower energy, in molecule **1** (421 nm) and **4–7** (370−470 nm), do not appear neither in the donor (PhOx[36] and Cz[37]) nor in the acceptor (BzN[38]) absorption spectra. Therefore, and in agreement with DFT calculations (Figure 4), they are assigned to the several singlet CT transitions occurring between the D and A moieties. More precisely, we can assign the CT band at a lower energy (between 421 and 467 nm) to PhOx CT and the ones at a higher energy (between 385 and 411 nm) to Cz CT. In compounds **5, 6**, and **7** containing additional Cz, it is possible to spot an additional shoulder (see Table 2) that can be assigned to the CT states resulting from the various Cz substituted at distinct positions on the BzN core. At higher energy (up to 360 nm), the absorption spectrum is almost entirely formed by superposition of the absorption of individual donors and acceptors. In particular, the absorption band at 287−289 nm, present only in compounds **4–7**, is assigned to the π−π* localized absorption of Cz.[37] The absorption bands between 324 and 330 nm are also associated with the localized absorption of Cz,[37] whereas the other absorption bands are assigned to the localized absorption of PhOx.[36]

*Table 2*: High and low energy absorption maximum wavelengths of **1** and **4**-**7** in cyclohexane (c=$10^{-5}$ M).

| **Compound** | **$\lambda_{max}$/ nm (LE)** | **$\lambda_{max}$ /nm (CT)** |
|---|---|---|
| **1** | 312, 297, 280(s) | 421 |
| **4** | 368(s), 324, 311, 301(s) 287, 277(s) | 426, 385 |
| **5** | 325, 302, 312, 287, 278(s) | 432, 391, 378(s) |
| **6** | 327, 316, 304 (s), 287 | 440, 404, 388(s) |
| **7** | 339, 330, 320, 289 | 467, 411, 373(s) |

(s) = shoulder

The absorption spectra of molecules of the 2nd and 3rd series in cyclohexane and PMMA are presented in Figure S6. These two series present a fully similar UV−vis absorption behavior as their parent compounds of the 1st series. Emission Properties.

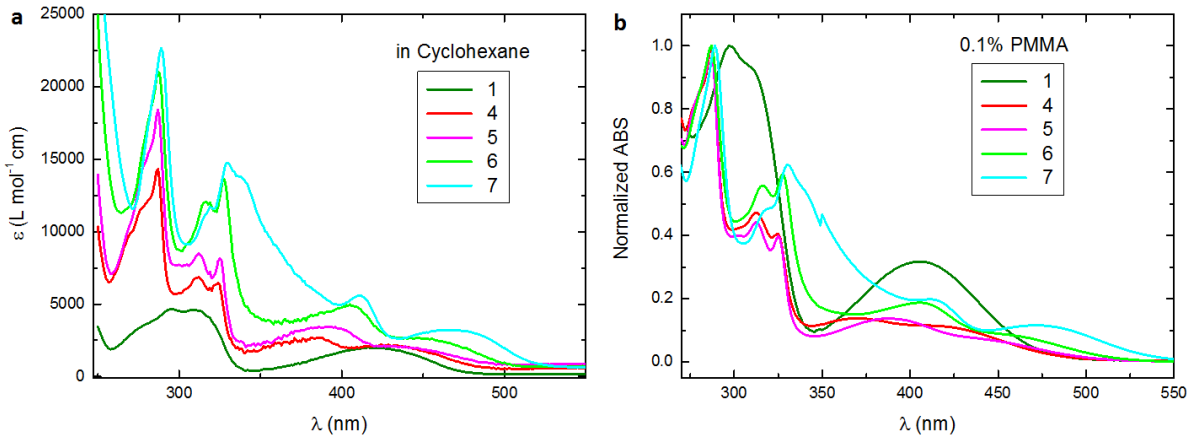


***Figure 5**:* Absorption spectra of **1** and **4-7** in **a)** cyclohexane ($10^{-5}$ M) and **b)** PMMA (0.1%wt). Absorption spectra in PMMA are normalized vs. the maximal absorbance value.

*Calculated Excited States.* A more detailed analysis of the TDDFT results done on both singlet and triplet states (Table S4) shows the presence of several excited states close in energy. The lower excited states correspond to the PhOx CT for both spin multiplicities. The corresponding calculated singlet to triplet energy gaps $\Delta E_{S-T}$ for **1–12** are reported in Table S5 and are typically small (0.04−0.20 eV) which should be beneficial for observing TADF. In the case of the compounds containing Cz substituents, there is also a relatively low-lying Cz CT that is found approximately 0.5 eV above the PhOx CT for both spin multiplicities. The $\Delta E_{S-T}$ values for these Cz CT states (see Table S5 for compounds **4–7**) are slightly larger than for the PhOx CT states but still remain rather small (0.16−0.20 eV). Finally, there are various LE states centered on either PhOx or BzN. In their singlet states, they are found 1.2 eV above the Phox CT but the triplet state is highly stabilized and one of these 3LE states is typically found close to the $^3$Cz CT. This low-lying triplet LE state should help the intersystem crossings (ISC and rISC). Scheme 4 presents the calculated energy levels of the singlet and triplet LE and CT states of compound **4** as a representative example of the series.

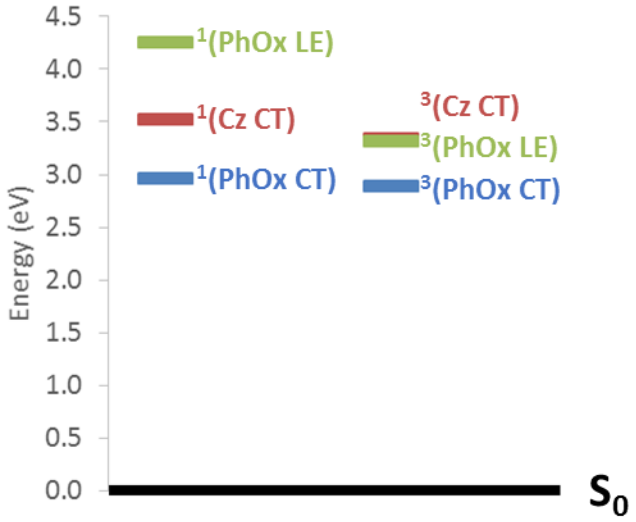


***Scheme 4:*** Calculated energy levels (left: singlets and right: triplets) involved in the emission properties of compound **4**.

*Experimental Emission Spectra.* The emission properties of the investigated compounds have been measured in solution and in PMMA films. The results are shown in Figure 6 (full spectra) and Figure S7 (high-energy bands) and data are reported in Table 3 for the 1st series. Remarkably, a dual emission is particularly evident for the molecules of the 1st series in cyclohexane (Figure 6a), an effect already reported by Karpiuk and Zhou[39,40] but not for TADF active compounds. In particular, **1** displays a very weak emission in the red region, assigned to the PhOx CT transition. The well-resolved emission in the blue region of **1** (387, 407, 425 s), (Figure S7a), is assigned to PhOx LE.[41] For molecules **4–7**, the emission band at low energy due to PhOx CT41 becomes much more intense. On the other hand, in **4** and **5**, the emission at higher energy appears only partially resolved. This is assigned to the sum of both PhOx LE and Cz CT contributions. With the increasing number of Czs (**6–7**), the emission at higher energy appears Gaussian without any vibronic resolution (Figure S7a). The remaining dual Gaussian emission can be associated exclusively to Cz CT (higher energy) and to PhOx CT (lower energy). From these observations, we understand that up to 2 Cz units, both PhOx LE and Cz CT contribute to the high-energy emission, whereas when the molecule is substituted with 3 or 4 Cz units, Cz CT becomes predominant. This behavior could depend on the occurrence of FRET between PhOx LE and Cz−BzN arms. Moreover, increasing the number of Cz leads to a stronger absorption of the Cz CT states, facilitating energy transfer from the PhOx LE making the emission from this latter to completely vanish.

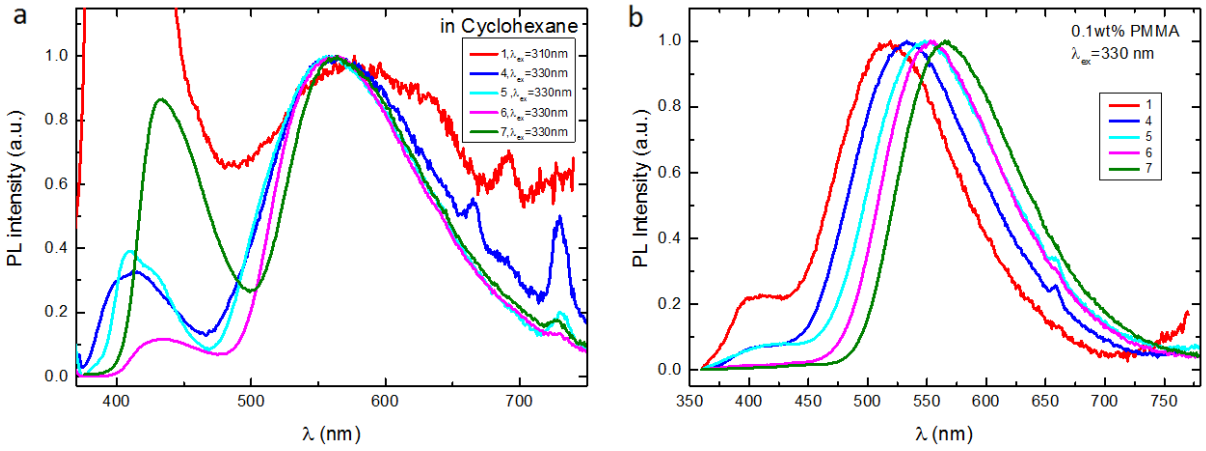


***Figure 6****:* Normalized (to the maxima of the PhOX CT band) photoluminescence spectra of **1** and **4**-**7** in a) cyclohexane (c=$10^{-5}$ M) and b) PMMA (0.1%wt). Excitation wavelength: 330 nm.

***Table 3:*** Experimental photoluminescence (PL) emission wavelengths for the first series.

| Compound | PL, $\lambda_{max}$ /nm[a] | | PL, $\lambda_{max}$/nm[b] |
|---|---|---|---|
| **1** | 387, 407, 425(s) | 577 | 578 |
| **4** | 404(s), 412 | 563 | 565 |
| **5** | 410, 423(s) | 556 | 559 |
| **6** | 432 | 565 | 565 |
| **7** | 432 | 564 | 564 |

[a] $\lambda_{ex}$ = 300-330 nm, [b] $\lambda_{ex}$ = 390-440 nm, (s)=shoulder

Excitation spectra have been recorded and are reported in Figure S8. The excitation matches the absorption in all cases, confirming that dual emission does not involve impurities but are actually associated to the excited states of the investigated compounds. Excitation spectra at emission wavelengths corresponding to PhOx and Cz CT states are also reported for compounds containing two different donors. Once again, these excitation spectra match pretty well with the absorption ones.

In PMMA, the PL band at low energy remains strong for all molecules (Figure 6b). On the contrary, the band at higher energy appears weak or even hardly visible and drastically decreases with the increasing number of Cz (Figure S7b), indicating that most of the excitation goes directly to the PhOx CT state. The reason for this behavior might be related to the rigid environment of the polymer host that reduces the mobility of Cz, which cannot rotate anymore to stabilize the Cz CT state.[24]

In order to evaluate the single-component white-light properties, the chromaticity coordinates were calculated for PL spectra of **4**–**7** (Figure S9a, Table S6). The obtained color coordinates change from warm-white to cold-white light and thus this class of molecules can be considered as potentially suitable for white-light display applications.

As regarding the emission properties of 2nd and 3rd series, they show a quite different behavior. The PL spectra are displayed in Figure S10. At a lower energy (between 480 and 750 nm), all molecules present a strong emission arising from PhOx CT, whereas at a higher energy (between 350 and 500 nm) emission is hardly visible in most cases. In particular, emission from PhOx LE is visible in **2** (Figure S10a, inset a) and becomes stronger in **3** (Figure S10c). On the other hand, emission from Cz CT is intense only in **12** (Figure S10c) and barely visible in other molecules (insets in Figure S10a,c). In our opinion, this is related to the higher number of PhOxs present in the 2nd and 3rd series that favors the emission from the PhOx CT state, so that all the excitation energy is transferred on this low-lying energy state.

From the steady-state absorption and emission properties, it is thus possible to conclude that in the three series, there is a gradual bathochromic shift of the CT absorption maximum with the increasing number of Czs (Figures 5 and S5). A bathochromic shift of the PL spectra occurs in PMMA for all three series, but only for the 2nd and 3rd series in solution (Figures 7, S7, S10). The bathochromic shift with the increasing number of Cz was already reported in the literature[42,43] and is related to the delocalization of the CT state that increases with the number of donors.

We can also conclude that depending on the number of Cz and on the surrounding medium, emission can stem from either BzN-Cz or BzN-PhOx CT states.

*Solvatochromism.* The photophysical properties of **4**–**7** were also investigated in three solvents with increasing polarity: cyclohexane ($\varepsilon$ = 2.0, $\mu$ = ~0.0 D); toluene ($\varepsilon$ = 2.4, $\mu$ = 0.36 D), and dichloromethane ($\varepsilon$ = 8.9, $\mu$ = 1.6 D). Positive solvatochromism was observed for both CT emission bands of all molecules (Figure 7). This effect further confirms that the dual emission of 4–7 in cyclohexane originates from two different CT states. Positive solvatochromism of the lowerenergy PhOx CT band is present for all molecules of the 2$^{nd}$ and 3rd series (Figure S11). On the other hand, the band at higher energy clearly visible in **3** is not affected by the solvent polarity, as suggested by its assignment to the PhOx LE.

*Effect of Oxygen on Quantum Yields and Lifetimes.* The PLQY ($\Phi_{PL}$) under air-equilibrated and deoxygenated conditions were measured in cyclohexane, toluene, and PMMA (Tables 4 and S7). In cyclohexane, two different excitation wavelengths were used, one relative to the absorption region of the donor and acceptor moieties ($\lambda$ex = 300−330 nm) and the other relative to the CT state absorption ($\lambda$ex = 390−430 nm).

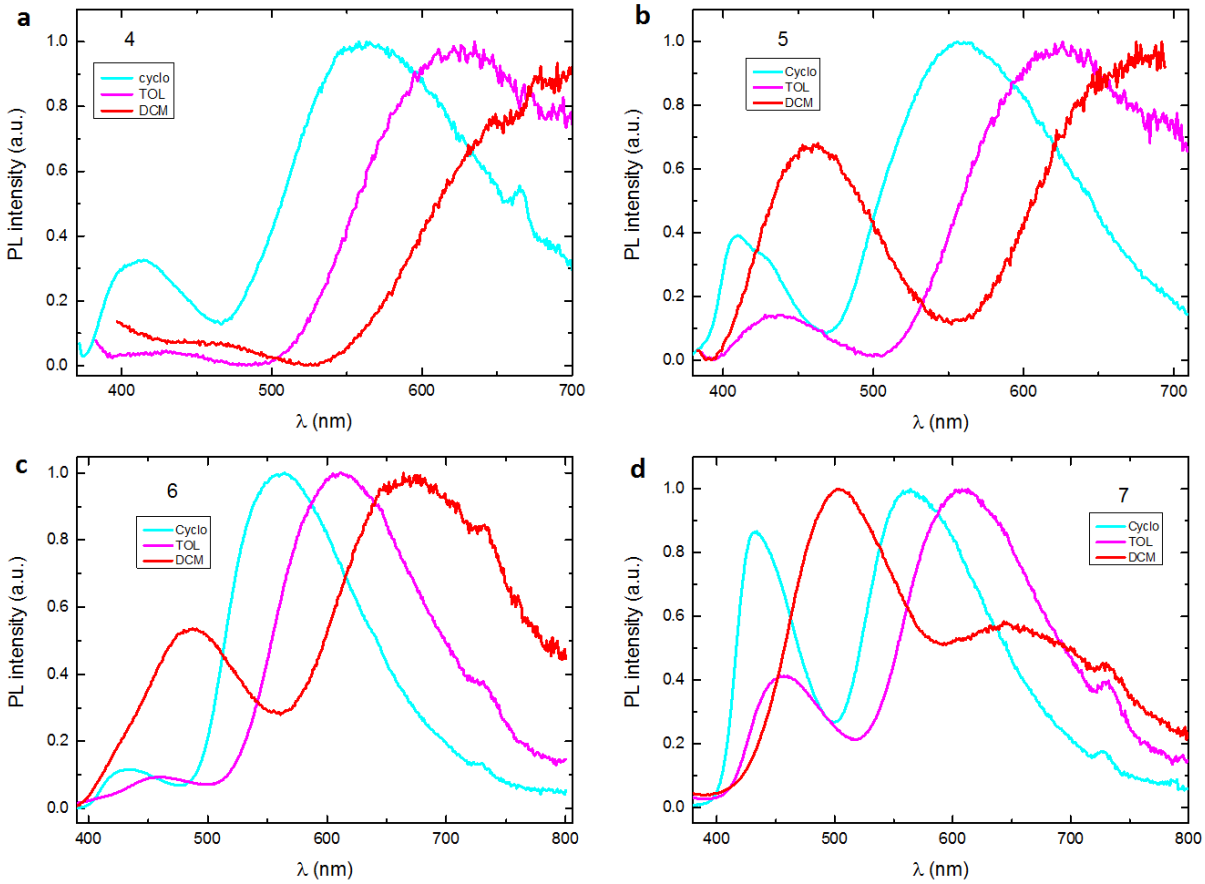


***Figure 7**:* Normalized photoluminescence (PL) spectra in cyclohexane ($10^{-5}$ M, cyan), toluene ($10^{-5}$ M, pink), and DCM ($10^{-5}$ M, red) of compounds **a) 4**, **b) 5**, **c) 6** and **d) 7.** Excitation wavelength: 330 nm.

Aerated PLQYs measured in cyclohexane increase with the number of substituents in the 1st and 2nd series, with the exception of the fully substituted compounds (**7, 10**). Conversely, in the 3rd series, PLQYs decrease with the number of substituents. The observed trend results from a balance between, on one hand, the positive effect of the CT state stabilization and, on the other hand, the activation of roto-vibrational non-radiative pathways, both effects occurring when increasing the number of donors. Finally, for the fully substituted compounds the non-radiative pathways become dominant and over-compete the CT stabilization effect. In toluene, PLQYs remain always very low and are not further discussed because differences between them may be smaller than the experimental errors. In PMMA, PLQYs tend to increase with the number of substituents except in the case of **1, 4**, and **5** where they remain similar. In a rigid matrix, the roto-vibrational non-radiative pathways are less favorable and the more substituted compounds are the most emissive thanks to the CT state stabilization.

After degassing the samples, all molecules experience a moderate increase of the PLQY (Tables 4 and S7) both in solution and PMMA films, which is indicative of a TADF activity. The PLQY of 4−7 in deoxygenated cyclohexane increases by a factor that depends on the excitation wavelength used, thus indicating that **4−7** exhibit TADF properties from both CT states. The spectra (Figure S12) clearly show that both emission bands increase in intensity after solvent deoxygenation when maintaining the same shape and position. The clear peak inversion between Cz CT and PhOx CT emissions after deoxygenating the cyclohexane solution of **7** indicates that TADF is more intense in the former than in the latter. For the

molecules of the 2nd and 3rd series (Figure S13), in all cases an increase of the PhOx CT emission intensity after degassing is observed. This confirms a TADF process associated to this transition. However, the PLQY obtained when exciting at 330 nm is similar to the one obtained at 400 nm (Table S7). This is in line with the fact that in the 2nd and 3rd series, the contribution of Cz CT to the total emission is weaker than in the 1st series.

***Table 4**:* Photoluminescence yield $\Phi_{PL}$ (%) of **1** and **4-7** in cyclohexane (CH), toluene and PMMA, with oxygen and after degassing.

| Compound | CH[a] | CH degas.[a] | CH[b] | CH degas.[b] | Toluene[a] | Toluene degas.[a] | PMMA[c] | PMMA degas.[c] |
|---|---|---|---|---|---|---|---|---|
| **1** | 0.2 | 0.2 | nd | Nd | - | - | 4.5 | 5.0 |
| **4** | 0.7 | 1.0 | 0.7 | 1.0 | - | - | 4.3 | 5.2 |
| **5** | 1.3 | 2.0 | 1.5 | 1.7 | 0.1 | 0.1 | 4.0 | 4.9 |
| **6** | 2.4 | 3.0 | 1.9 | 2.1 | 0.3 | 0.3 | 13.6 | 15.9 |
| **7** | 1.6 | 2.5 | 1.3 | 1.7 | 0.2 | 0.2 | 15.1 | 18.1 |

[a] $\lambda_{ex}$=300-330 nm, [b] $\lambda_{ex}$=390-430 nm, [c] $\lambda_{ex}$=400 nm, nd: not detected (too weak)

Finally, the ratio of DF to prompt fluorescence (PF) could also be obtained from the emission PLQYs measured in air saturated and degassed cyclohexane solutions (Table 5). We have estimated the DF over PF ratio using steady-state experiments, owing to the fact that TADF is typically quenched by oxygen, whereas PF is not. The small DF/PF obtained for the 1st series indicates a poor contribution of TADF in solution. On the contrary, the DF/PF values are larger in the 2nd and 3rd series which demonstrates that a higher number of PhOx units help enhance TADF properties in this class of materials. This is in line with the stronger donor effect of PhOx, which is generally used to improve the TADF properties of D−A compounds.[44,45]

***Table 5**:* Delayed fluorescence (DF) vs. prompt fluorescence (PF) ratio values.

| | | DF/PF |
|---|---|---|
| **1st series** | **1** | - |
| | **4** | 0.62 |
| | **5** | 0.68 |
| | **6** | 0.59 |
| | **7** | 0.67 |
| **2nd series** | **2** | 1.14 |
| | **8** | 0.93 |
| | **9a** | 1.17 |
| | **10** | 1.18 |
| **3rd series** | **3** | 1.21 |
| | **11** | 0.54 |
| | **12** | 0.91 |

In order to further confirm the TADF properties of these compounds, PL decays were collected and lifetimes measured (Table 6). The decays comprise two to three characteristic lifetimes: one in the nanosecond regime attributed to the PF and one or two in the microsecond range due to TADF. It is interesting to note that the compounds displaying two long lifetimes are the same that present two emission bands.

***Table 6:*** Luminescence lifetimes of molecules **1**-**12** in cyclohexane at RT recorded in absence of oxygen.

| Series | Compound | $\tau 1_{av}$ (ns) | τ2(ns) | τ3(ns) | $\tau_{av}$ (µs) |
|---|---|---|---|---|---|
| 1st | **1** | n.e. | n.e. | n.e. | n.e. |
| | **4** | 14.7 ±0.10 | 384 ±2.8 (99%) | 2162 ±40 (1%) | 1.9 |
| | **5** | 8.9 ±0.06 | 1200 ±10 (96%) | 8828 ±59 (4%) | 8.6 |
| | **6** | 8.2 ±0.01 | 1599 ±12 (91%) | 14403 ±61 (9%) | 11.4 |
| | **7** | 17.8 ±0.10 | 1459 ±100 (87%) | 24291 ±200 (13%) | 23.7 |
| 2nd | **2** | 17.2 ±0.30 | 715 ±21 | - | 0.7 |
| | **8** | 19.8 ±0.07 | 824 ±19 | - | 0.8 |
| | **9a** | 17.3 ±0.20 | 585 ±13 | - | 0.6 |
| | **10** | 13.74 ±0.30 | 343 ±1.8 (99%) | 2330 ±4.5 (1%) | 2.3 |
| 3rd | **3** | 18.8 ±0.20 | 651 ±30 | - | 0.7 |
| | **11** | 11.7 ±0.10 | 673 ±5.3 | - | 0.7 |
| | **12** | 3.2 ±0.03 | 574 ±11 (99%) | 1092 ±3.6 (1%) | 1.0 |

n.e. not emissive

In order to better understand the origin of the two long lifetimes, the PL decays of **7** have been recorded at two different emission wavelengths corresponding to the maximum of the two emission bands (440 and 560 nm). The results are displayed in Figures 8 and S14. In addition to the expected PF short lifetime (17.8 ns), three longer ones have been extracted, 24 µs (at 440 and 560 nm), 1.5 µs (440 nm), and 0.7 µs (560 nm). In Figure 8 it is possible to see that decays collected at different emission wavelengths present two long components. However, when the decay is collected at 440 nm which corresponds to the emission maximum of Cz CT, the contribution of the longer DF (24 µs) is higher compared to the decay collected at 560 nm (emission maximum of PhOx CT). Conversely, at this latter wavelength, the shorter DF component presents a higher contribution. This behavior indicates that Cz CT is the one that lives longer and can be related to the higher increase of the Cz CT emission band in degassed cyclohexane compared to the PhOx CT one. The different behaviors of the Cz and PhOx emission decays are consistent with their different magnitudes of TADF contributions (Figure 8). These facts suggest that the

Cz and PhOx CT states (singlet and triplet) are independent from each other and do not communicate through ISC or FRET.

To summarize, a general kinetic scheme showing all the photophysical processes involved was built with the help of the fluorescence and TDDFT results (Scheme 5). We can see that after the absorption, the PF (kPF) emission could arise from LE (PhOx) and/or both CT states (involving Cz or PhOx). On the other hand, the DF ($k_{DF}$) only arises from the CT states. The non-radiative decay ($k_{nr}$) is quite important for this class of materials, especially for the ones showing low PLQY.

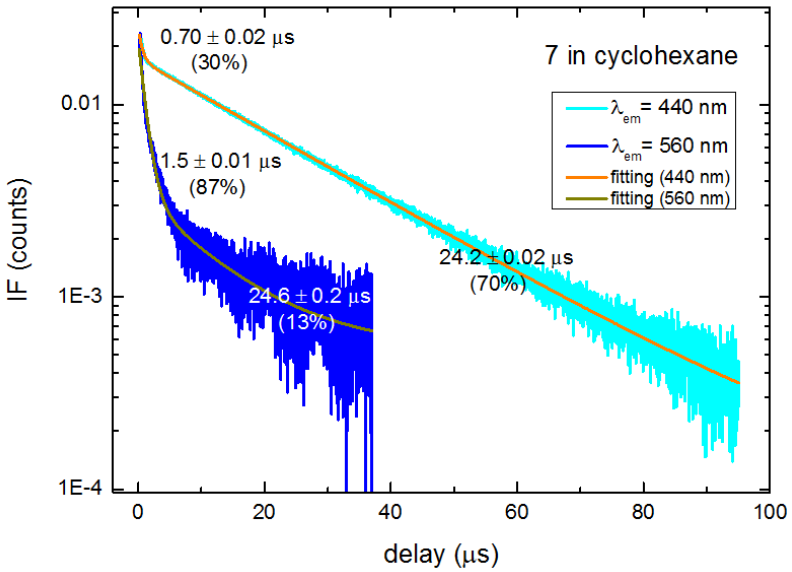


***Figure 8:*** Fluorescence decays (µs regime) of **7** in cyclohexane, collected on the emission maximum of CT Cz (light blue) or CT PhOx (dark blue). Decays were recorded in the absence of oxygen. Excitation wavelength: $\lambda_{exc}$=355 nm.

**CONCLUSIONS**

We have synthesized a whole family of new compounds presenting dual emission from two CT states as well as TADF emission properties. The DFT calculations show that electronically excited CT states of different energies can be formed when molecules contain both Cz and PhOx donors. Beyond the typical local emission of donor and acceptor moieties, these molecules are characterized by the presence of a double CT emission involving Cz and PhOx, respectively, mainly in solution. Moreover, especially for the 1st series, the results strongly suggest that the Cz and PhOx CT states are independent from each other. The CT emission involving Cz is more intense in the 1st series, particularly for molecules containing a larger number of Czs. The double emission, especially observed in the 1st series leads to chromaticity coordinate values that vary from warm-white to cold-white, thus demonstrating that this class of molecules can be considered as potentially highly suitable for white-light display applications. Moreover, a gradual bathochromic shift with the increasing number of substituents was observed in all three series, both in absorption and in solid-state emission, leading to a fine tuning of the color emission. Increasing the number of Cz units improves the solid-state PLQY, up to 18% in PMMA films. Conversely, fluorescence yields remain rather low in solution. Moreover, it was demonstrated that increasing the

number of PhOx units helps to improve the TADF properties in this class of materials, in line with the stronger donor properties of PhOx compared to Cz.

Besides the photophysical properties, we have also observed intriguing electrochemical behaviors for these compounds. We have demonstrated the sequential oxidation of PhOx and Cz units in agreement with their relative donor strength. More importantly, we propose a mechanism explaining the (polyfluoro)benzonitrile irreversible reduction. We believe that the fluoride anion acts as a leaving group in the anion radical formed upon electron uptake, but the fluorine expulsion only occurs after dimerization, provided that the number of substituents remains small. In the other cases, a reversible reduction is observed showing that the anion radical formed remains stable.

In conclusion, the dual emission developed by using two different donors can be considered as a promising strategy: (i) to tune the emission color by properly selecting the parent molecules, and (ii) to achieve white luminescence for lighting applications. In fact, we hope that this work should help single white-light-emitting organic TADF molecules become prominent in future display and lighting applications.

## ASSOCIATED CONTENT

Supporting Information

The Supporting Information is available free of charge at

https://pubs.acs.org/doi/10.1021/acs.jpcb.2c00219.

Synthesis protocols, NMR and mass spectra, XRD analysis, DFT calculations, electrochemistry, UV−vis absorption spectra, and emission spectra (PDF)

## ACKNOWLEDGMENTS

The research leading to these results received funding from the European Union's Horizon 2020 research and innovation program under the Marie Skłodowska-Curie grant agreement no. 674990 (EXCILIGHT). This work was performed using HPC resources from the "Mésocentre" computing center of CentraleSupélec and École Normale Supérieure Paris-Saclay supported by CNRS and Région Île-de-France (http://mesocentre.centralesupelec.fr/) and HPC resources of CINES under the allocation 2018-A0050810547 made by GENCI. Vincenzo Maiorano (CNR Nanotec Lecce) is warmly acknowledged for giving access to the experimental setup for additional experiments.

## REFERENCES

(1) Kido, J.; Kimura, M.; Nagai, K. Multilayer White Light-Emitting Organic Electroluminescent Device. Science 1995, 267, 1332−1334.

(2) Sun, Y.; Giebink, N. C.; Kanno, H.; Ma, B.; Thompson, M. E.; Forrest, S. R. Management of Singlet and Triplet Excitons for Efficient White Organic Light-Emitting Devices. Nature 2006, 440, 908−912.

(3) Yang, Q.-Y.; Lehn, J.-M. Bright White- Light Emission from a Single Organic Compound in the Solid State. Angew. Chem., Int. Ed. 2014, 53, 4572−4577.

(4) Kim, S. H.; Park, S.; Kwon, J. E.; Park, S. Y. Organic Light-Emitting Diodes with a White-Emitting Molecule: Emission Mechanism and Device Characteristics. Adv. Funct. Mater. 2011, 21, 644−651.

(5) Daub, J.; Engl, R.; Kurzawa, J.; Miller, S. E.; Schneider, S.; Stockmann, A.; Wasielewski, M. R. Competition between Conformational Relaxation and Intramolecular Electron Transfer within Phenothiazine-Pyrene Dyads. J. Phys. Chem. A 2001, 105, 5655–5665.

(6) Etherington, M. K.; Franchello, F.; Gibson, J.; Northey, T.; Santos, J.; Ward, J. S.; Higginbotham, H. F.; Data, P.; Kurowska, A.; Dos Santos, P. L.; Graves, D. R.; Batsanov, A. S.; Dias, F. B.; Bryce, M. R.; Penfold, T. J.; Monkman, A. P. Regio- and Conformational Isomerization Critical to Design of Efficient Thermally-Activated Delayed Fluorescence Emitters. Nat. Commun. 2017, 8, 14987.

(7) Etherington, M. K.; Gibson, J.; Higginbotham, H. F.; Penfold, T. J.; Monkman, A. P. Revealing the Spin-Vibronic Coupling Mechanism of Thermally Activated Delayed Fluorescence. Nat. Commun. 2016, 7, 13680.

(8) Penfold, T. J. On Predicting the Excited-State Properties of Thermally Activated Delayed Fluorescence Emitters. J. Phys. Chem. C 2015, 119, 13535–13544.

(9) Dias, F. B.; Bourdakos, K. N.; Jankus, V.; Moss, K. C.; Kamtekar, K. T.; Bhalla, V.; Santos, J.; Bryce, M. R.; Monkman, A. P. Triplet Harvesting with 100% Efficiency by Way of Thermally Activated Delayed Fluorescence in Charge Transfer Oled Emitters. Adv. Mater. 2013, 25, 3707–3714.

(10) Gibson, J.; Monkman, A. P.; Penfold, T. J. The Importance of Vibronic Coupling for Efficient Reverse Intersystem Crossing in Thermally Activated Delayed Fluorescence Molecules. ChemPhysChem 2016, 17, 2956–2961.

(11) Dias, F. B.; Penfold, T. J.; Monkman, A. P. Photophysics of Thermally Activated Delayed Fluorescence Molecules. Methods Appl. Fluoresc. 2017, 5, 012001.

(12) Kalinowski, J.; Cocchi, M.; Virgili, D.; Fattori, V.; Williams, J. A. G. Mixing of Excimer and Exciplex Emission: A New Way to Improve White Light Emitting Organic Electrophosphorescent Diodes. Adv. Mater. 2007, 19, 4000–4005.

(13) Hung, W. Y.; Fang, G. C.; Lin, S. W.; Cheng, S. H.; Wong, K. T.; Kuo, T. Y.; Chou, P. T. The First Tandem, All-Exciplex-Based Woled. Sci. Rep. 2014, 4, 5161.

(14) Jankus, V.; Chiang, C.-J.; Dias, F.; Monkman, A. P. Deep Blue Exciplex Organic Light-Emitting Diodes with Enhanced Efficiency; PType or E-Type Triplet Conversion to Singlet Excitons? Adv. Mater. 2013, 25, 1455–1459.

(15) Uoyama, H.; Goushi, K.; Shizu, K.; Nomura, H.; Adachi, C. Highly Efficient Organic Light-Emitting Diodes from Delayed Fluorescence. Nature 2012, 492, 234–238.

(16) Cho, Y. J.; Yook, K. S.; Lee, J. Y. High Efficiency in a Solution-Processed Thermally Activated Delayed-Fluorescence Device Using a Delayed-Fluorescence Emitting Material with Improved Solubility. Adv. Mater. 2014, 26, 6642–6646.

(17) Cho, Y. J.; Chin, B. D.; Jeon, S. K.; Lee, J. Y. 20% External Quantum Efficiency in Solution-Processed Blue Thermally Activated Delayed Fluorescent Devices. Adv. Funct. Mater. 2015, 25, 6786–6792.

(18) Cho, Y. J.; Jeon, S. K.; Chin, B. D.; Yu, E.; Lee, J. Y. The Design of Dual Emitting Cores for Green Thermally Activated Delayed Fluorescent Materials. Angew. Chem., Int. Ed. 2015, 54, 5201–5204.

(19) Cho, Y. J.; Jeon, S. K.; Lee, J. Y. Molecular Engineering of High Efficiency and Long Lifetime Blue Thermally Activated Delayed Fluorescent Emitters for Vacuum and Solution Processed Organic Light-Emitting Diodes. Adv. Opt. Mater. 2016, 4, 688–693.

(20) Park, I. S.; Lee, S. Y.; Adachi, C.; Yasuda, T. Full-Color Delayed Fluorescence Materials Based on Wedge-Shaped Phthalonitriles and Dicyanopyrazines: Systematic Design, Tunable Photophysical Properties, and Oled Performance. Adv. Funct. Mater. 2016, 26, 1813–1821.

(21) Tanimoto, S.; Suzuki, T.; Nakanotani, H.; Adachi, C. Thermally Activated Delayed Fluorescence from Pentacarbazorylbenzonitrile. Chem. Lett. 2016, 45, 770–772.

(22) Zhang, D.; Cai, M.; Zhang, Y.; Zhang, D.; Duan, L. Sterically Shielded Blue Thermally Activated Delayed Fluorescence Emitters with Improved Efficiency and Stability. Mater. Horiz. 2016, 3, 145–151.

(23) Matsuo, K.; Yasuda, T. Blue Thermally Activated Delayed Fluorescence Emitters Incorporating Acridan Analogues with Heavy Group 14 Elements for High-Efficiency Doped and Non-Doped Oleds. Chem. Sci. 2019, 10, 10687–10697.

(24) Aydemir, M.; Xu, S.; Chen, C.; Bryce, M. R.; Chi, Z.; Monkman, A. P. Photophysics of an Asymmetric Donor-Acceptor-Donor Tadf Molecule and Reinterpretation of Aggregation-Induced TADF Emission in These Materials. J. Phys. Chem. C 2017, 121, 17764–17772.

(25) Xu, S.; Liu, T.; Mu, Y.; Wang, Y.-F.; Chi, Z.; Lo, C.-C.; Liu, S.; Zhang, Y.; Lien, A.; Xu, J. An Organic Molecule with Asymmetric Structure Exhibiting Aggregation-Induced Emission, Delayed Fluorescence, and Mechanoluminescence. Angew. Chem. Int. Ed. 2015, 54, 874–878.

(26) Xie, Z.; Chen, C.; Xu, S.; Li, J.; Zhang, Y.; Liu, S.; Xu, J.; Chi, Z. White-Light Emission Strategy of a Single Organic Compound with Aggregation-Induced Emission and Delayed Fluorescence Properties. Angew. Chem., Int. Ed. 2015, 54, 7181–7184.

(27) Zhao, J.; Chen, X. J.; Yang, Z.; Liu, T. T.; Yang, Z. Y.; Zhang, Y.; Xu, J. R.; Chi, Z. G. Highly-Efficient Doped and Nondoped Organic Light-Emitting Diodes with External Quantum Efficiencies over 20% from a Multifunctional Green Thermally Activated Delayed Fluorescence Emitter. J. Phys. Chem. C 2019, 123, 1015–1020.

(28) Huang, L.; Wen, X.; Liu, J.; Chen, M.; Ma, Z.; Jia, X. An Aie Molecule Featuring Changeable Triplet Emission between Phosphorescence and Delayed Fluorescence by an External Force. Mater. Chem. Front. 2019, 3, 2151–2156.

(29) Yang, Z.; Mao, Z.; Xu, C.; Chen, X.; Zhao, J.; Yang, Z.; Zhang, Y.; Wu, W.; Jiao, S.; Liu, Y.; et al. A Sterically Hindered Asymmetric D-a-D ' Thermally Activated Delayed Fluorescence Emitter for Highly Efficient Non-Doped Organic Light-Emitting Diodes. Chem. Sci. 2019, 10, 8129–8134.

(30) Huang, J.; Nie, H.; Zeng, J.; Zhuang, Z.; Gan, S.; Cai, Y.; Guo, J.; Su, S.-J.; Zhao, Z.; Tang, B. Z. Highly Efficient Nondoped OLEDs with Negligible Efficiency Roll-Off Fabricated from Aggregation-Induced Delayed Fluorescence Luminogens. Angew. Chem., Int. Ed. 2017, 56, 12971–12976.

(31) Karon, K.; Lapkowski, M. Carbazole Electrochemistry: A Short Review. J. Solid State Electrochem. 2015, 19, 2601–2610.

(32) Savéant, J. M.; Costentin, C. Elements of Molecular and Biomolecular Electrochemistry: An Electrochemical Approach to Electron Transfer Chemistry, 2nd ed.; Wiley, 2000; p P100.

(33) Asirvatham, M. R.; Hawley, M. D. Mechanism of Dimer Formation in Electroreduction of Para-Fluorobenzonitrile. J. Am. Chem. Soc. 1975, 97, 5024–5026.

(34) Nielsen, M. F.; Utley, J. H. P. Organic Electrochemistry; Hammerich, O., Lund, H., Eds.; Marcel Dekker, 2000; p 867.

(35) Farnham, W. B. Fluorinated Carbanions. Chem. Rev. 1996, 96, 1633–1640.

(36) Vanallan, J. A.; Reynolds, G. A.; Adel, R. E. Polynuclear Heterocycles .1. 1h-Benzo B Pyridol 1,2,3-Mn Phenoxazin-1-1 and Related Substances. J. Org. Chem. 1962, 27, 1659–1664.

(37) Bonesi, S. M.; Erra-Balsells, R. Electronic Spectroscopy of Carbazole and N- and C-Substituted Carbazoles in Homogeneous Media and in Solid Matrix. J. Lumin. 2001, 93, 51–74.

(38) Hirt, R. C.; King, F. T. Search for Weak Absorption Bands of Benzonitrile in the near Ultraviolet. J. Chem. Phys. 1952, 20, 1821–1822.

(39) Karpiuk, J. Dual Fluorescence from Two Polar Excited States in One Molecule. Structurally Additive Photophysics of Crystal Violet Lactone. J. Phys. Chem. A 2004, 108, 11183–11195.

(40) Zhou, H.; Mei, J.; Chen, Y.-A.; Chen, C.-L.; Chen, W.; Zhang, Z.; Su, J.; Chou, P.-T.; Tian, H. Phenazine-Based Ratiometric $Hg^{2+}$ Probes with Well-Resolved Dual Emissions: A New Sensing Mechanism by Vibration-Induced Emission (Vie). Small 2016, 12, 6542–6546.

(41) Santos, P. L.; Ward, J. S.; Data, P.; Batsanov, A. S.; Bryce, M. R.; Dias, F. B.; Monkman, A. P. Engineering the Singlet-Triplet Energy Splitting in a TADF Molecule. J. Mater. Chem. C 2016, 4, 3815–3824.

(42) Tanaka, H.; Shizu, K.; Nakanotani, H.; Adachi, C. Twisted Intramolecular Charge Transfer State for Long-Wavelength Thermally Activated Delayed Fluorescence. Chem. Mater. 2013, 25, 3766–3771.

(43) Xie, F.-M.; Zhou, J.-X.; Li, Y.-Q.; Tang, J.-X. Effects of the Relative Position and Number of Donors and Acceptors on the Properties of Tadf Materials. J. Mater. Chem. C 2020, 8, 9476–9494.

(44) Tanaka, H.; Shizu, K.; Miyazaki, H.; Adachi, C. Efficient Green Thermally Activated Delayed Fluorescence (Tadf) from a Phenoxazine-Triphenyltriazine (Pxz-Trz) Derivative. Chem. Commun. 2012, 48, 11392–11394.

(45) Borowicz, P.; Herbich, J.; Kapturkiewicz, A.; Opallo, M.; Nowacki, J. Radiative and Nonradiative Electron Transfer in Donor–Acceptor Phenoxazine and Phenothiazine Derivatives. Chem. Phys. 1999, 249, 49–62.

(46) Frisch, M. J.; Schlegel, H. B.; Scuseria, G. E.; Robb, M. A.; Cheeseman, J. R.; Scalmani, G.; Barone, V.; Petersson, G. A.; Nakatsuji, H.; et al. Gaussian 16, Revision B.01; Gaussian, Inc.: Wallingford CT, 2016.

(47) O'Boyle, N. M.; Tenderholt, A. L.; Langner, K. M. Cclib: A Library for Package-Independent Computational Chemistry Algorithms. J. Comput. Chem. 2008, 29, 839–845.

(48) Würth, C.; Grabolle, M.; Pauli, J.; Spieles, M.; Resch-Genger, U. Relative and Absolute Determination of Fluorescence Quantum Yields of Transparent Samples. Nat. Protoc. 2013, 8, 1535–1550.